Journal of Alloys and Compounds 522 (2012) 78–84

Contents lists available at SciVerse ScienceDirect

Journal of Alloys and Compounds

journal homepage: www.elsevier.com/locate/jallcom

Microstructure, tensile properties and creep behaviors of as-cast Mg–2Al–1Zn–*x*Gd (*x* = 1, 2, 3, and 4 wt.%) alloys

Xudong Wang, Wenbo Du*, Ke Liu, Zhaohui Wang, Shubo Li

School of Materials Science and Engineering, Beijing University of Technology, Beijing 100124, China

ARTICLE INFO

Article history:
Received 1 July 2011
Received in revised form 11 January 2012
Accepted 16 January 2012
Available online 28 January 2012

Keywords:
Microstructure
Gadolinium
Tensile property
Creep behavior

ABSTRACT

The microstructure, tensile properties and creep behaviors of as-cast Mg–2Al–1Zn–*x*Gd (*x* = 1, 2, 3, and 4 wt.%) alloys have been investigated. The results indicated that the addition of Gd led to the formation of a branched $(Mg, Al)_3Gd$ phase and a cubic Al_2Gd phase. The tensile properties of the AZ21 alloy have been improved greatly at both room temperature and elevated temperature due to the presence of the branched $(Mg, Al)_3Gd$ phase. The AZ21 alloy containing 4% Gd presented a good creep-resistant property. The steady-region and the total creep strain of the alloy after 100 h were 2.6×10^{-8} s^{-1} and 1.2%, respectively. The enhancement of creep properties of the AZ21 alloy was mainly ascribed to the thermal stable branched $(Mg, Al)_3Gd$ phase by which the movement of dislocations were impeded effectively.

1. Introduction

Currently, a great interest in the development of light alloy materials which generally have excellent mechanical properties due to a result of stricter requirements on the greenhouse gas emissions and fuel economy in vehicles have been attracted [1]. The Mg-based alloys usually exhibit notable attractiveness to the automotive industry as structural parts due to low densities and high specific strength [2]. In all of the magnesium alloys, the Mg–Al–Zn series alloys have the most wide spread application. The Mg–Al–Zn alloys can offer a good combination of mechanical properties, corrosion resistance and castability, but the use of these alloys at present is limited mainly due to the inferior heat resistance properties, especially the creep resistance property compared with aluminum alloys at high temperature [3]. For example, the AZ91D alloy tends to lose its creep strength above 150 °C [4]. So, it loses commercial value in application when it is used as structural parts at 150 °C. Therefore, one of the most important investigations on magnesium alloys is to develop an alloy which can be economically applied at the temperatures up to 200 °C [5,6].

The reason for poor heat-resistant properties of the Mg–Al–Zn series alloys is mainly ascribed to the existence of the β-$Mg_{17}Al_{12}$ phase. Therefore, in order to improve the performance of the Mg–Al–Zn series alloys at high temperature, it is necessary to suppress the formation of the β-$Mg_{17}Al_{12}$ phase [7]. Thus, one of the most important ways to improve the heat resistance of the alloys is alloying with other elements. It has been reported that additions of RE elements into the Mg alloys were an effective approach to attain good creep properties at high temperature [8]. Furthermore, it was found that the Mg–Gd series alloys had better mechanical properties than the other commercial magnesium alloys. It is well known that the solid solubility of the Gd in the Mg matrix drops greatly with temperature decreasing. As reported by Gao et al. [9], the solid solution strengthening effect of Gd and Y was much higher than that of the Al and Zn. Besides, Peng et al. [10] reported that the peak-ageing hardened Mg–8Gd–0.6Zr–3Er alloy exhibited good ultimate tensile strength (UTS) and yield strength (YS) after peak ageing treatment, the values of which were 261 and 173 MPa at room temperature, respectively. Apart from that, the values of the UTS and YS of the peak-ageing Mg–8Gd–0.6Zr–3Er alloy were 203 and 122 MPa at 250 °C, respectively. It was considered that the improvement of the peak hardness and mechanical properties of the Mg–Gd series alloys were mainly attributed to the fine dispersed metastable β-$Mg_{15}RE_3$ (Gd/Er) phase and the β-Mg_5RE (Gd/Er) precipitate. Yin et al. [11] reported that the peak-aged Mg–11.4Gd–2.2Nd–0.45Zr alloy not only displayed high UTS of 307 MPa with an elongation of 1.4% at room temperature but also presented its high strength of more than 260 MPa at 300 °C, which was mainly attributed to the solid solution strengthening and precipitates strengthening. On the basis of previous investigations, it has been shown that the Gd additions have a great effect on improving the heat-resistant properties via forming kinds of precipitates. However, the amount of RE added into such Mg alloys is too high to have possibility of wide spread application. Furthermore, published researches concerning the effects of RE elements on microstructure and mechanical properties of the most popular commercial wrought AZ series alloys are

* Corresponding author. Tel.: +86 1 67392917; fax: +86 1 67392917.
E-mail address: duwb@bjut.edu.cn (W. Du).

0925-8388/$ – see front matter © 2012 Elsevier B.V. All rights reserved.
doi:10.1016/j.jallcom.2012.01.084

Table 1
The chemical compositions of the alloys A, B, C, D and AZ21 alloys (wt.%).

Alloys	Al	Zn	Gd	Mg
A	2.1	1.0	1.1	Bal.
B	2.2	1.1	1.9	Bal.
C	2.0	1.0	2.9	Bal.
D	2.1	1.1	3.8	Bal.
AZ21	2.2	1.0	–	Bal.

limited. Therefore, in the present work the effects of the Gd additions on the microstructure, mechanical properties, heat resistance and creep deformation mechanism of an Mg–2Al–1Zn alloy were investigated. Meantime, the relationship between microstructure and mechanical properties were also discussed.

2. Experimental procedures

The experimental alloys with nominal compositions of Mg–2Al–1Zn–1Gd (alloy A), Mg–2Al–1Zn–2Gd (alloy B), Mg–2Al–1Zn–3Gd (alloy C) and Mg–2Al–1Zn–4Gd (alloy D) were prepared from a high purity Mg (>99.95%), Al (>99.95%), Zn (>98.5%) and Mg–30Gd (wt.%) master alloy melted in a graphite crucible under a mixed atmosphere of N_2 and SF_6 by using an electric resistance furnace. The melting alloy liquid was stirred to ensure a homogeneous composition, held at 770 °C for ~30 min, and then cast into a permanent mould. The cast ingot with a size of 33 mm × 100 mm was cooled down at air atmosphere.

The chemical compositions of the alloys were determined by an X-ray fluorescence (XRF) analyzer (Magic PW2403), as show in Table 1. The phase constituents of the alloys were analyzed by X-ray diffraction (XRD, D8 ADVANCE) measurements in the 2θ scanning range 20–80° with a 0.02° step size. A scanning electron microscope (SEM, HITACHI S-450) and a transmission electron microscope (TEM, JEM-2100, JEOL) equipped with energy dispersive spectroscopy (EDS) were used to observe the microstructure of the alloys. The specimens for SEM observation were sliced from the same position of each casting. They were polished and then etched with a solution of 5 ml nitric acid + 95 ml ethyl alcohol. The specimens for TEM observation were prepared first by electro-polishing and finally polished by ion beam milling. The electro-polishing of the samples was conducted in a solution of 20% nitric acid and 80% methanol, using a liquid nitrogen cold region to keep the temperature at −25 °C. The ion beam milling performed at an incident angle less than 10°.

Cylindrical tensile specimens of 5 mm in gauge diameter and 25 mm in gauge length (shown schematically in Fig. 1) were machined from the bulk as-cast ingots. The tensile tests at elevated temperature were performed on a tensile test machine with a temperature control system. The samples were heated by an electric resistance furnace and kept at the required temperature for 5 min prior to be tensile tested. A set of three tensile tests was conducted for all conditions [12]. The creep tests were carried out on a css-3902 creep tester under a constant load of 50 MPa for100 h at 200 °C, and the elongations in all creep curves were calculated by subtracting the immediate strain from the total elongation in order to eliminate the possibility of some slip inside the grip. The microstructures of the specimens after creep test were observed by using TEM.

3. Experimental results

3.1. Microstructure

3.1.1. Effect of Gd on microstructures of the cast alloys

The microstructures of the as-cast alloys have been investigated. The XRD patterns and SEM micrographs of the as-cast alloys A, B, C and D are shown in Figs. 2 and 3, respectively. It is indicated that the microstructure of each as-cast alloys is very similar except the volume fraction of the main secondary phase. One of the main phase

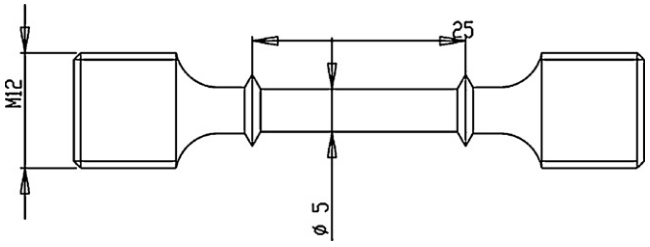

Fig. 1. Shape and size of a creep sample (mm).

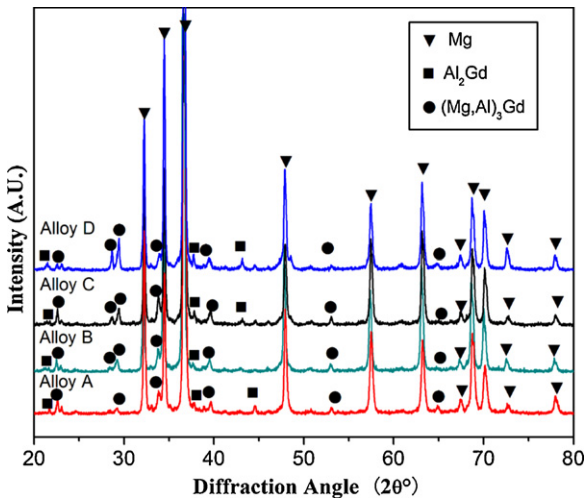

Fig. 2. XRD patterns of the as-cast alloys A, B, C and D.

components is the α-Mg solid solution which contains a solute of Zn. The EDS result shows that the α-Mg matrix contains 0.69 wt.% Zn. The SEM and XRD analyses reveal that two kinds of secondary phases are present in the AZ21alloys containing Gd. One is the branched phase with a lamellar morphology, as shown in Fig. 3, which is mainly located within the interdendritic interstices. The other is a few of particles with angular morphology, as shown in Fig. 3(f), which are distributed within the matrix. As suggested by Fig. 3, the microstructures of the investigated alloys mainly consist of the highly branched (Mg, Al)$_3$Gd phase while the as-cast AZ21 alloy mainly contains the island-like $Mg_{17}Al_{12}$ phase, as shown in Fig. 3(h). As illustrated in Figs. 2 and 3, the formation of the $Mg_{17}Al_{12}$ phase was suppressed by the addition of Gd.

With an increase in the content of Gd, the volume fractions of the two kinds of the intermetallic phases increases [13,14]. As shown in Fig. 3, the volume fractions of the main secondary phases in the Mg–2Al–1Zn–4Gd alloy are probably twice as many as that in the Mg–2Al–1Zn–1Gd alloy.

3.1.2. Effect of Gd on the formation of secondary phases

In order to identify the crystalline structure of the intermetallic compounds in the as-cast alloys, TEM, HREM and selected area diffraction (SAED) observations have been performed.

Fig. 4(a) shows a bright field TEM image of an example of angular particles in the as-cast Mg–2Al–1Zn–3Gd alloy. The EDS result and corresponding SAED pattern with the electron beam parallel to the [$\bar{1}$ 1 2] zone obtain from the particles are shown in Table 2 and Fig. 4(b), respectively. The EDS result shows that the particle are mainly composed of Al and Gd, and the ratio (at.%) of Al/Gd is ~2.2:1 [15]. All of the results obtained were consistent with the C15-type Laves phase of Al_2Gd with a lattice constant of 7.917 Å [16]. Fig. 5 shows a representative bright-field TEM image together with the corresponding EDS, SAED pattern and HREM image of the lamellar phase obtained from the sample of the Mg–2Al–1Zn–3Gd

Table 2
The EDS results of the Al_2Gd phase.

	Al K	Gd L
EDS result 1	68.93	31.07
EDS result 2	70.31	29.69
EDS result 3	65.08	34.92
EDS result 4	68.54	31.46

Average $Al^{at.\%}/Gd^{at.\%}$ = 2.2:1.

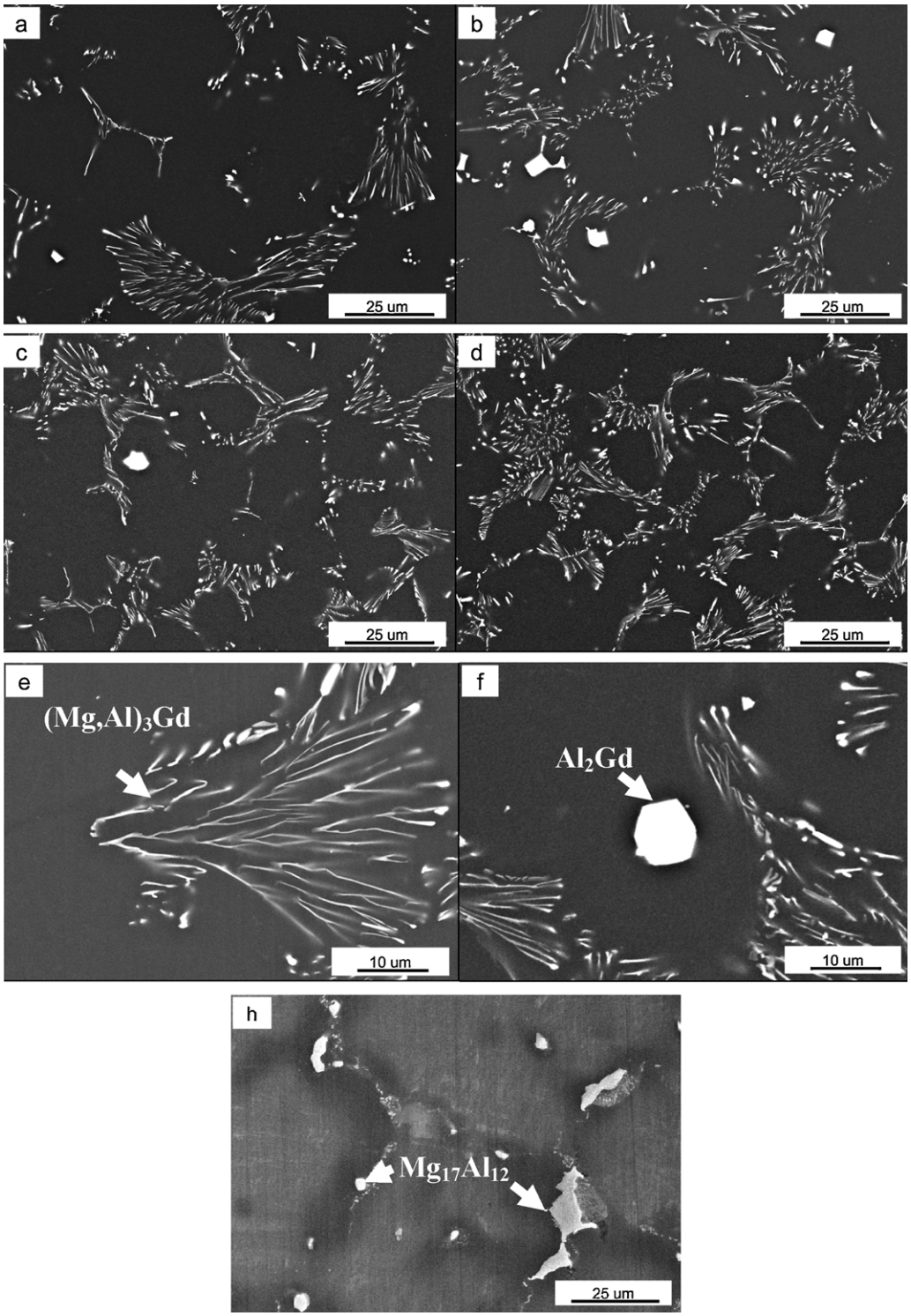

Fig. 3. SEM images of the as-cast alloys A, B, C and D: (a) alloy A, (b) alloy B, (c) alloy C, (d) alloy D, (e) the branched (Mg, Al)$_3$Gd phase in the alloy C, (f) the angular Al_2Gd phase in the alloy C and (h) as-cast AZ21 alloy.

alloy. The EDS equipped in TEM reveals that the average composition of the lamellar phases lies between 69.13–72.96 (Mg, Al) and 27.04–30.87Gd (at.%). Therefore, the eutectic compound can be described as (Mg, Al)$_3$Gd. The detailed HREM image and the corresponding SAED pattern with the electron beam parallel to the [0 0 1] zone and [1 0 0] zone are also presented. The HREM image result and SAED pattern are consistent with an Mg_3Cd-type compound belonging to the space group of *P*63/*mmc* (no. 194). The cell parameters of the (Mg, Al)$_3$Gd phase are $a = b = 0.722$, $c = 0.573$ nm, $\alpha = \beta = 90^\circ$, $\lambda = 120^\circ$ and the cell volume = 0.259 nm^3.

3.2. Tensile properties

In order to better understand the strengthening mechanisms of the as-cast Mg–2Al–1Zn–*x*Gd (x = 1, 2, 3, and 4 wt.%) alloys, the volume fraction of the (Mg, Al)$_3$Gd phase was calculated. According

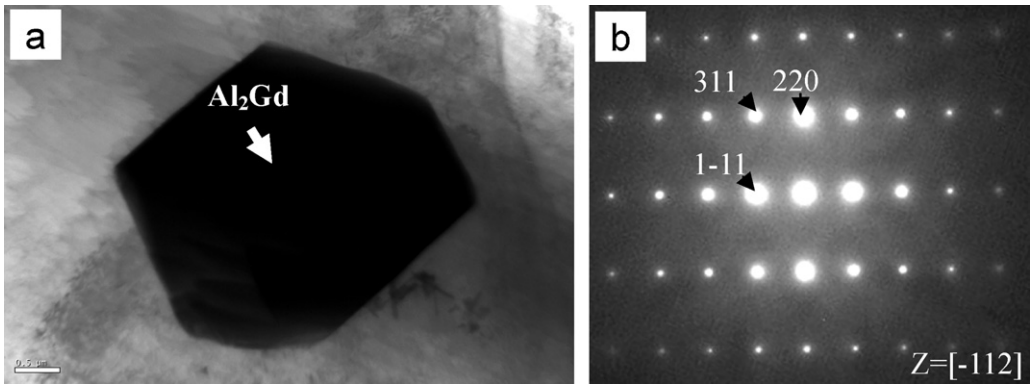

Fig. 4. TEM bright field images and corresponding SAED patterns taken from the angular Al_2Gd phase in the alloy C: (a) TEM bright image and (b) corresponding SAED pattern.

to the previous investigations [17,18], the volume fraction of the $(Mg, Al)_3Gd$ phase in the alloys can be described as the below relationship:

$$V_{p1} = \frac{m_1/\rho_1}{m_1/\rho_1 + (1 - m_1)\rho_m} \quad (1)$$

where ρ_1 and m_1 are the densities and mass fractions of $(Mg, Al)_3Gd$, respectively, on the assumption that all the Al atoms are inclined to form the $(Mg, Al)_3Gd$ phase except the Al atoms which are dissolved in the matrix, and ρ_m is the density of matrix. The density of the precipitated phase is calculated by following equation:

$$\rho_p = \sum_j \frac{n_j W_j}{D_P} \quad (2)$$

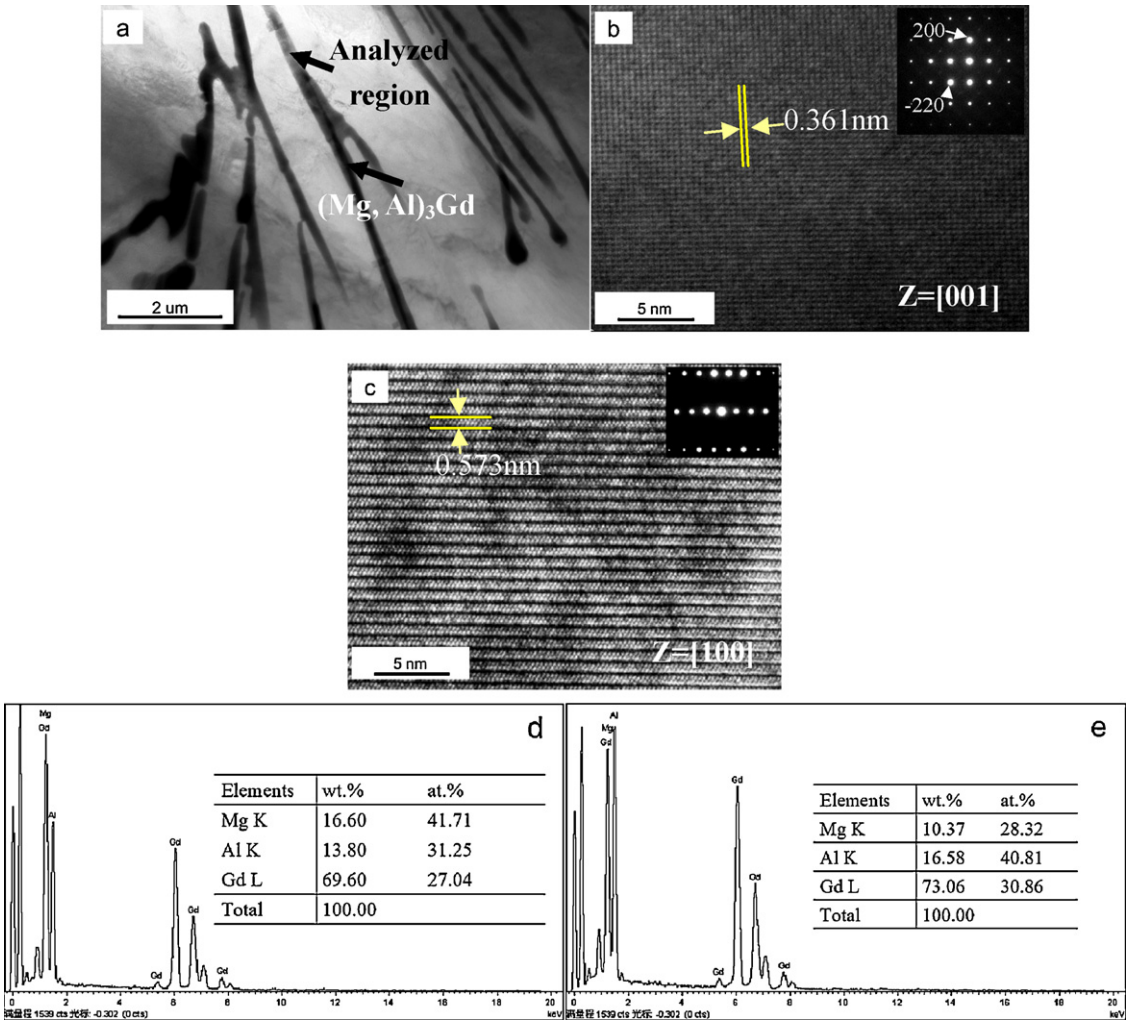

Fig. 5. TEM bright field images, HREM, EDS and SAED pattern taken from the branched $(Mg, Al)_3Gd$ phase in the alloy C: (a) TEM bright image, (b) and (c) HREM and SAED patterns with the electron beam parallel to the [0 0 1] zone and [1 0 0] zone, respectively, (d) and (e) corresponding EDS.

Table 3
The tensile properties of the as-cast alloys A, B, C and D at RT and 200 °C.

Alloys	RT			200 °C		
	UTS (MPa)	YS (MPa)	*E* (%)	UTS (MPa)	YS (MPa)	*E* (%)
A	213	102	12.5	111	71	23.6
B	235	118	11.4	126	80	21.2
C	249	123	9.4	130	86	17.3
D	242	133	8.4	140	90	15.9

where D_P is the volume of the crystal cell of the precipitated phase, and n_j and W_j are the number and quality of the j atom in the crystal cell of the precipitated phase, respectively. The crystal cells of $(Mg, Al)_3Gd$ ($a = b = 0.722$ nm, $c = 0.573$ nm, $\alpha = \beta = 90°$, $\lambda = 120°$, cell volume = 0.259 nm^3) phase were calculated according to the TEM and HREM results.

According to relationships (1) and (2), the volume fractions of $(Mg, Al)_3Gd$ phases in as-cast Mg–2Al–1Zn–*x*Gd ($x = 1$, 2, 3, and 4 wt.%) alloys are calculated, i.e. 1.12, 1.89, 2.52, and 3.01%, respectively. The calculated results indicate that the $(Mg, Al)_3Gd$ phase is the main strengthening phase in the as-cast Mg–2Al–1Zn–*x*Gd ($x = 1$, 2, 3, and 4 wt.%) alloys.

The tensile properties of the alloys at RT and at 200 °C are given in Table 3. It can be seen that both the yield strength (YS) and the ultimate tensile strength (UTS) are improved with an increase in Gd content either at room temperature (RT) or at elevated temperature. At RT, the Mg–2Al–1Zn–4Gd alloy shows the highest YS among all the investigated alloys, but the elongation is the lowest. It indicates that the increase in the volume fraction of the $(Mg, Al)_3Gd$ ternary phase increases the yield strength while it is converse to the elongation of the alloy [19]. Similarly, at 200 °C, the Mg–2Al–1Zn–4Gd alloy also displays the highest YS and UTS. It is suggested that the Mg–2Al–1Zn–4Gd alloy has a better thermal stability. On the whole, the tensile strength of the alloys decreases as the temperature increases. Conversely, the elongation of the alloys increases with the increment of the temperature.

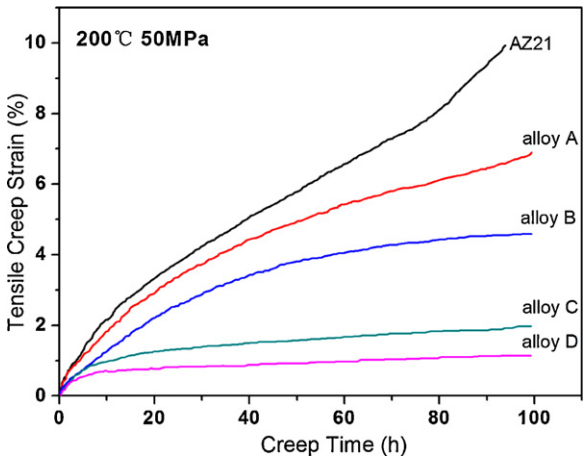

Fig. 6. Creep test curves of the as-cast alloys A, B, C and D at 200 °C and a constant load of 50 MPa.

3.3. Creep tests

The tensile creep curves of the as-cast alloys A, B, C, D and AZ21 alloy under a constant load of 50 MPa at 200 °C for 100 h are shown in Fig. 6. The creep curves observed includes only two creep regions for all the alloys except for the AZ21 alloy within the time period of the test. The first is a short primary region, and the second is a prolonged steady-state region [20,21]. Moreover, it is apparently found that the tertiary creep region has not been initiated even after 100 h, which is indicated that the Mg–2Al–1Zn–*x*Gd alloys have excellent creep-resistant attributes. By examining the total strain during creep test, it can be seen that the total creep strain of the alloy D decreases to a minimum value, which is reached in approximately one seventh of the time 100 h compared to alloy A. The creep rate at the steady-region and the total creep strain after 100 h for the alloy D are 2.6×10^{-8} s^{-1} and 1.2%, respectively, whereas the steady-region and total creep strain after 100 h for AZ21are

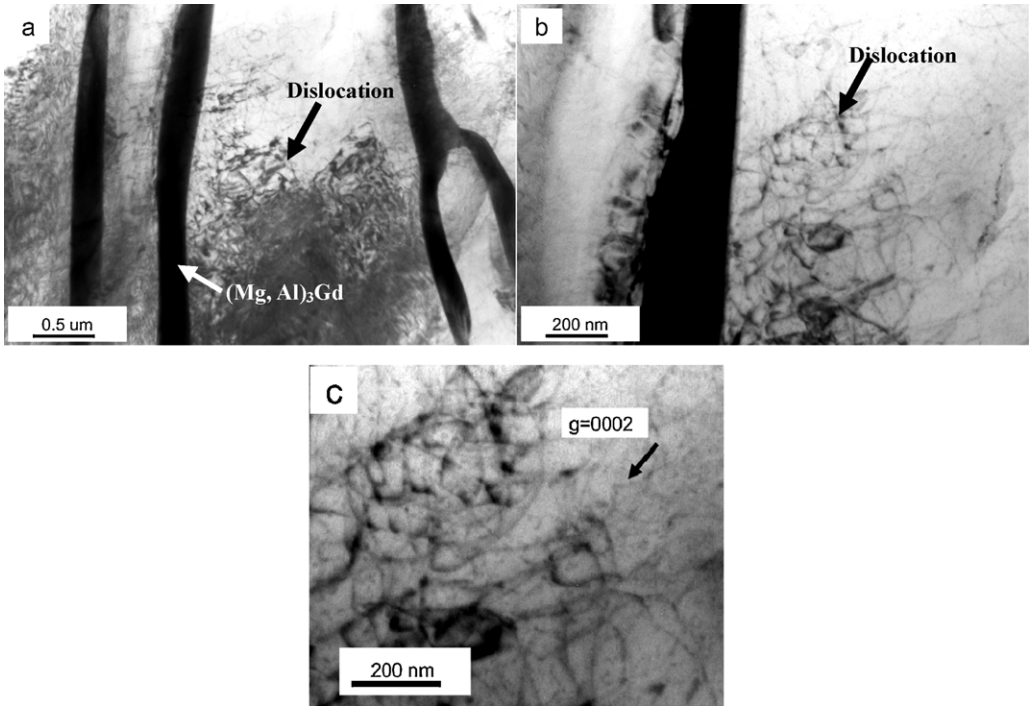

Fig. 7. (a and b) The dislocation structures and (c) the interaction between the dislocations and the precipitates in the Mg–2Al–1Zn–4Gd alloy after creep test at 200 °C with a load of 50 MPa for 100 h.

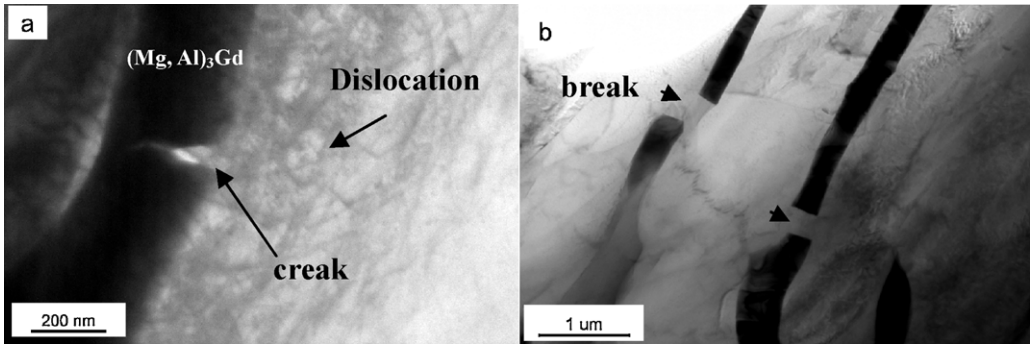

Fig. 8. (a) The crack formed by a high density of dislocations and (b) the broken lamellae phase in the Mg–2Al–1Zn–2Gd alloy after creep test under the creep conditions of 200 °C and 50 MPa for 100 h.

$30 \times 10^{-8}\ s^{-1}$ and 9.7%, respectively. Meanwhile, the minimum creep rate for the alloy AE42 is $10.6 \times 10^{-8}\ s^{-1}$ under a constant load of 60 MPa at 200 °C [22]. However, the creep rate for the alloy B is $\sim 11.3 \times 10^{-8}\ s^{-1}$. The results indicate that the alloy AZ21 containing Gd has an excellent high-temperature creep-resistant performance, and the minimum creep rate tents to decrease with an increase in the Gd content.

3.4. Post-crept microstructure

In order to understand the mechanism responsible for the improvement in the creep resistance of the alloys with Gd addition, the microstructures of the alloys after creep test were investigated by TEM. Fig. 7 shows TEM images obtained from the as-cast Mg–2Al–1Zn–4Gd alloy after creep under a load of 50 MPa at 200 °C for 100 h. A large numbers creep-induced dislocations occur between the lamellae phase of the $(Mg, Al)_3Gd$, as shown in Fig. 7(a). Moreover, the $(Mg, Al)_3Gd$ phase is so stable that it does not decompose even after prolonged exposure (100 h) under the test creep conditions of 200 °C and 50 MPa. Fig. 7(b) shows that the interaction between the dislocations and the $(Mg, Al)_3Gd$ phase, where it can be seen that the dislocations are blocked by the $(Mg, Al)_3Gd$ phase (as indicated by the arrows). In Fig. 7(c), the incident beam direction is aligned parallel to the basal plane, so that the dislocation of the basal-slip system aligned parallel to the basal plane trace are straight. Therefore, the dislocations are in the non-basal slip systems in the present crept specimens [23].

4. Discussion

Magnesium has an hcp structure and only three active slip systems exist [5]. Therefore, grain boundary sliding is regarded as a major creep mechanism of magnesium alloys below 175 °C. But the relatively better elongation to failure obtained from the Mg–2Al–1Zn–1Gd alloy seems to be different from that stated above. Fig. 8(a) shows that a crack appears at the inner of the lamellars of the $(Mg, Al)_3Gd$ phase under the stress concentration in the alloy Mg–2Al–1Zn–2Gd during creep test. Fig. 8(b) shows that the cracks have appeared in the lamellars phase of $(Mg, Al)_3Gd$ in the Mg–2Al–1Zn–1Gd alloy. As suggested by the TEM investigation, the creep-induced dislocations are mobile dislocations on non-basal planes in the present crept specimens [24]. It leads to a better creep elongation of the Mg–2Al–1Zn–1Gd alloy during creep test [25]. Generally speaking, the cross slips of the non-basal mobile dislocations plays an important role in improving the creep resistance behaviors of the Mg–2Al–1Zn–*x*Gd alloys [26].

The present investigation shows that the addition of Gd into the Mg–2Al–1Zn alloy leads to a significant alteration in the microstructures, which directly result in an increase of the creep resistance of the alloys at 200 °C. The results imply that the addition Gd is an effective method to strengthen the AZ series alloys against creep deformation. In conclusion, the formation of the $(Mg, Al)_3Gd$ compound is considered to be responsible for the higher creep resistance performance of the alloys. The reasons for the improvement in the heat resistance can be summarized below: (1) the addition of Gd to the Mg–2Al–1Zn alloys could suppress the formation of the β-$Mg_{17}Al_{12}$ phase, which tends to decompose at elevated temperature, due to the preferential reaction between the aluminium atoms and Gd atom [27]. Furthermore, the chances of creep-induced precipitation of the $Mg_{17}Al_{12}$ phase and the diffusion of solute atoms of aluminum at elevated temperature are greatly reduced [28]. (2) Compared with the microstructures of the $(Mg, Al)_3Gd$ phase before the creep test, no obvious changes of microstructures of the $(Mg, Al)_3Gd$ phase are observed after the creep test. It indicates that the $(Mg, Al)_3Gd$ phase remains stable during the creep test [25]. It has been reported that the $Al_{11}RE_3$ compound will be decomposed to Al_2RE and the $Mg_{17}Al_{12}$ phases during creep test in AE42 alloy. Whereas no such changes in microstructure of the $(Mg, Al)_3Gd$ compound have been observed in the Mg–2Al–1Zn–*x*Gd alloys [28,29]. Therefore, it is apparently found that the $(Mg, Al)_3Gd$ compound is more thermally stable than that of the $Al_{11}RE_3$ and the β-$Mg_{17}Al_{12}$ phases. (3) According to the results, it is suggested that the glide of the non-basal dislocation controls the creep behaviors of the alloys in our investigation. The $(Mg, Al)_3Gd$ phase can effectively impede the dislocation motion [28].

5. Conclusions

The investigation of the microstructures, tensile properties and creep behaviors of the as-cast Mg–2Al–1Zn–*x*Gd (x = 1, 2, 3, and 4 wt.%) alloys have been investigated. The following conclusions can be obtained.

(1) The microstructures of the investigated alloys are composed of dominant α-Mg solid solution with a content of Zn and $(Mg, Al)_3Gd$ phase as well as a tiny of Al_2Gd phase. The volume fraction of the $(Mg, Al)_3Gd$ phase increases with the content of Gd increases.
(2) The tensile experiments indicate that the branched $(Mg, Al)_3Gd$ phase can improve the mechanical properties of the AZ21 alloys significantly.
(3) The creep test results suggest that the heat resistance of the Mg–2Al–1Zn alloys at 200 °C could be obviously improved with the addition of Gd. The Mg–2Al–1Zn–4Gd alloy shows the best heat resistance among the present investigated alloys. The $(Mg, Al)_3Gd$ phase has a great effect on improving the creep resistance by impeding the movement of the dislocations.

Acknowledgements

This work was supported by National Key Basic Research Program (NKBRP) 2007CB613706, National Science and Technology Supporting Plan of the Twelve Five-year 2011BAE22B04-2, National Natural Science Fund of China (51071004) and the project of Innovation Project for Talents (PHR200906101).

References

[1] L. Shang, I.H. Jung, S. Yue, R. Verma, E. Essadiqi, J. Alloys Compd. 492 (2010) 173–183.
[2] K. Liu, J. Meng, J. Alloys Compd. 509 (2011) 3299–3305.
[3] D.H. Xiao, M. Song, F.Q. Zhang, Y.H. He, J. Alloys Compd. 484 (2009) 416–421.
[4] B.H. Kim, S.W. Lee, Y.H. Park, I.M. Park, J. Alloys Compd. 493 (2010) 502–506.
[5] M. Sumida, J. Alloys Compd. 460 (2008) 619–626.
[6] N.D. Nam, W.C. Kim, J.G. Kim, K.S. Shin, H.C. Jung, J. Alloys Compd. 509 (2011) 4839–4847.
[7] H. Liu, Y. Chen, Y. Tang, S. Wei, G. Niu, J. Alloys Compd. 440 (2007) 122–126.
[8] J. Wang, S. Gao, P. Song, X. Huang, Z. Shi, F. Pan, J. Alloys Compd. 509 (2011) 8567–8572.
[9] L. Gao, R.S. Chen, E.H. Han, J. Alloys Compd. 481 (2009) 379–384.
[10] Q. Peng, H. Dong, Y. Wu, L. Wang, J. Alloys Compd. 456 (2008) 395–399.
[11] D.D. Yin, Q.D. Wang, Y. Gaoa, C.J. Chen, J. Zheng, J. Alloys Compd. 509 (2011) 1696–1704.
[12] Q. Peng, J. Wang, Y. Wu, L. Wang, Mater. Sci. Eng. A 433 (2006) 133–138.
[13] J. Zhang, Z. Leng, S. Liu, M. Zhang, J. Meng, R. Wu, J. Alloys Compd. 509 (2011) L187–L193.
[14] J. Bai, Y.S. Sun, S. Xun, F. Xue, S. Xue, J. Qiang, T.B. Zhu, Mater. Sci. Eng. A 419 (2006) 181–188.
[15] M. Sumida, S. Jung, T. Okane, J. Alloys Compd. 475 (2009) 903–910.
[16] X. Tao, Y. Ouyang, H. Liu, F. Zeng, Y. Feng, Y. Du, Z. Jin, Comput. Mater. Sci. 44 (2008) 392–399.
[17] Y. Wu, W. Du, Z. Yan, Z. Wang, T. Zuo, Rare Metals 29 (2010) 55–61.
[18] Y.D. Huang, H. Dieringa, N. Hort, P. Maier, K.U. Kainer, Y.L. Liu, J. Alloys Compd. 463 (2008) 238.
[19] X. zheng, L. Wang, J. Wang, Y. Wu, Z. Ning, J. Sun, L. Wang, Mater. Sci. Eng. A 515 (2009) 98–101.
[20] K. Milička, F. Dobeš, J. Alloys Compd. 378 (2004) 167–171.
[21] J.J. Park, Int. J. Refract. Met. Hard Mater. 17 (1999) 331–337.
[22] H. Dieringa, N. Hort, K.U. Kainer, Mater. Sci. Eng. A 510–511 (2009) 382–386.
[23] S. Spigarelli, M. Cabibbo, E. Evangelista, M. Talianker, V. Ezersky, Mater. Sci. Eng. A 289 (2000) 172–181.
[24] J. Koike, T. Kobayashi, T. Mukai, H. Watanabe, M. Suzuki, K. Maruyama, K. Higashi, Acta Mater. 51 (2003) 2055–2065.
[25] H. Zou, X. Zeng, C. Zhai, W. Ding, Mater. Sci. Eng. A 392 (2005) 229–234.
[26] B. Smola, I. Stulíková, J. Pelcová, B.L. Mordike, J. Alloys Compd. 378 (2004) 196–201.
[27] Y. Lü, Q. Wang, X. Zeng, W. Ding, C. Zhai, Y. Zhu, Mater. Sci. Eng. A 278 (2000) 66–76.
[28] I.A. Anyanwu, Y. Gokan, A. Suzuki, S. Kamado, Y. Kojima, S. Takeda, T. Ishida, Mater. Sci. Eng. A 380 (2004) 93–99.
[29] I.P. Moreno, T.K. Nandy, J.W. Jones, J.E. Allison, T.M. Pollock, Scr. Mater. 48 (2003) 1029.